Reversible phase-change behavior in two-dimensional antimony telluride (Sb_2Te_3) nanosheets

Robin B. Jacobs-Gedrim,[1] Michael T. Murphy,[1] Fan Yang,[1] Nikhil Jain,[1] Mariyappan Shanmugam,[1] Eui Sang Song,[1] Yudhister Kandel,[1] Parham Hesamaddin,[2] Hong Yu Yu,[3] M. P. Anantram,[4] David B. Janes,[2] and Bin Yu[1,a)]

[1]*College of Nanoscale Science and Engineering, State University of New York, Albany, New York 12203, USA*
[2]*Department of Electrical and Computer Engineering, Purdue University, West Lafayette, Indiana 47907, USA*
[3]*Department of Electronic and Electrical Engineering, Southern University of Science and Technology, Shenzhen, Guangzhou 518052, People's Republic of China*
[4]*Department of Electrical Engineering, University of Washington, Seattle, Washington 98195, USA*

(Received 10 November 2017; accepted 8 March 2018; published online 26 March 2018)

Potential two-dimensional (2D) van der Waals crystals with mechanical flexibility, transparency, and low cost are viable material platforms for future nanodevices. Resistive switching behavior in 2D layered Sb_2Te_3 nanosheets is demonstrated. Nearly three orders of magnitude switch in sheet resistance were realized for more than 20 cycles. The observed hysteretic behavior is due to the change between crystalline and amorphous phases under a melt-quench-recrystallization mechanism. More importantly, the energy required to amorphize the nanosheets decreases exponentially with layer thickness reduction. It is expected that scaling to the ultimate two-dimensional limit in chalcogenide nanosheet-based phase change devices may meet or even exceed the energy efficiency of neurobiological architectures. *Published by AIP Publishing.* https://doi.org/10.1063/1.5013099

Resistive switching in layered materials molybdenum disulphide (MoS_2) has been studied.[1] By passing current through MoS_2, Joule heating had caused a temperature rise in the material to reach the low resistance phase. In 1968, Ovshinsky reported that this effect could be reversed by rapid heating and cooling under a melt-quench mechanism,[2] making the material suitable for memory implementation. As the extraction of atomic monolayers from layered bulk materials was proved to be possible (with the isolation of graphene) in 2004, the exploration efforts on a large number of two-dimensional (2D) materials, including TiO_2,[3] MoS_2,[3] WS_2,[3] and In_2Se_3 (Ref. 4), have been actively pursued. What's more, the prototypes of logic switches,[5] radio-frequency (RF) transistors,[6] interconnects,[7,8] solar cells,[9] and various types of sensors[10–12] have all been reported on 2D materials. While a key element in future electronic systems, non-volatile memory has not yet been found to be composed exclusively of a single 2D nanosheet.

Hereby, we demonstrate resistive switching behavior in 2D layered Sb_2Te_3 nanosheets. Antimony (III) telluride (Sb_2Te_3) is a layer-structured material with phase change properties suitable for applications in nonvolatile random access memory.[13] Due to crystalline-amorphous phase transitions under a melt-quench-recrystallization mechanism, the hysteretic behavior was observed and the on/off ratio in resistance was nearly three orders of magnitude for over 20 cycles. More importantly, we discovered that the energy required to amorphize the nanosheets would decrease exponentially with layer thickness reduction, indicating an extremely low power consumption when the scaling phase changes layered materials to the ultimate two-dimensional limit (In the Sb_2Te_3 material case, 1 nm for 1 quintuple layer). The discovery of resistive switching behavior in two-dimensional materials opens up the possibility of developing memory,[14] logic,[15] and synaptronics[16] with flexible manufacturing techniques and heterostructured designs.[3]

Device fabrication began with a 300 mm (100) Si wafer, which was oxidized on both sides to a depth of 100 nm. The oxide on the back of the wafer was etched away with hydrofluoric acid. A single step of UV photolithography was performed on the front side and developed before depositing a nominal 5 nm Ti/50 nm Au layer followed by liftoff to produce 50 μm × 50 μm contact pads separated by interdigitated electrodes. Where the nanosheets crossed the contacts and were suspended over a channel without contamination at the interface, an ohmic interface was formed ($R2 > 9.9$). Sb_2Te_3 (Alfa Aesar, 99.999% purity) was sourced in the form of 6 mm lumps. The lumps were cleaved with a razor blade to remove the outer surfaces which may have been contaminated with oxygen from the atmosphere. Next, nanosheets of Sb_2Te_3 were then extracted by micromechanical exfoliation and transferred onto the substrate with embedded interdigitated electrodes. It is noted that our group simultaneously works on the bottom-up deposition process for Sb_2Te_3, trying to realize memristors based on ultrathin Sb_2Te_3 nanoplates.[17,18] Optical Microscopy (Olympus, BX60MF5) and Scanning Electron Microscopy (SEM, FEI Dualbeam 600) were employed to determine the locations where a nanosheet crossed the raised contacts. The Scanning Electron Microscopy (SEM) images and the corresponding Atomic Force Microscopy (AFM) line-scans of several prepared nanosheets are shown in Figs. 1(a)–1(f). Different sizes and thicknesses of Sb_2Te_3 crystals were obtained suspending across the raised Ti/Au contacts. X-ray diffraction from an ensemble of Sb_2Te_3 nanosheets confirms that the crystal structure of nanosheets is hexagonally symmetric in space group RBm no. 166 with lattice constants $a = b = 4.26$ Å and $c = 30.458$ Å as shown in Fig. S1.[19]

a)Author to whom correspondence should be addressed: byu@sunypoly.edu

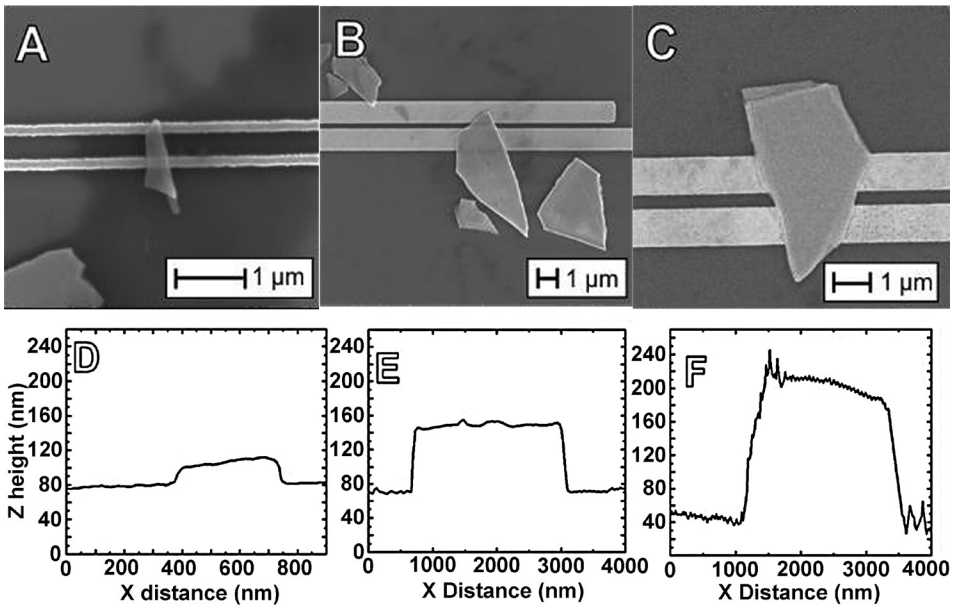


FIG. 1. (a)–(c) Scanning electron microscopy (SEM) images of the exfoliated Sb_2Te_3 nanosheets crossing two Ti/Au metal contacts. (d)–(f) AFM line-scans, taken along the bottom electrical contact and across the nanosheet, show the physical thickness.

The electrical measurements for the Sb_2Te_3 Phase Change Random Access Memory (PCRAM) devices were performed in a cryogenic/vacuum probe station (Lakeshore, CPX) with a semiconductor parameter analyzer (Agilent, B1500A) mainframe. The resistance of the device is measured by sweeping voltage and measuring current, calculated by initial I-V characteristics in Fig. 2(a). Initially, the nanosheets are in a crystalline phase that exhibits low electrical resistance and ohmic behavior at the metal contacts.

To assess the energy required for a RESET switch, a single pulse of 10 ns pico- watt (pW) and 10 ns edge time was performed with the device in the low-resistance state (LRS). The voltage during switching was measured in real time via an oscilloscope. When ultra-short voltage pulses of arbitrary polarity called RESET pulses are applied to the nanosheets, a dramatic decrease in conductivity is observed as shown in Fig. 2(b). Once in the high-resistance state, or HRS, the application of direct current can return the device to its original low-resistance state, or LRS, as shown in Fig. 2(c) by way of the negative differential resistance.[13] The application of the direct crystalline phase is thermo-dynamically favorable, and the phase reached via pulsing is metastable. After pulsing, the device was again measured with a low voltage I-V sweep, as shown in Fig. 2(d). The resultant high current indicates that the device has returned to a low resistance state. Besides switch behavior, it is noticed that the resistance is lower than the initial value [shown in Fig. 2(a)]. We attributed it to the contact annealing during current pulsing.

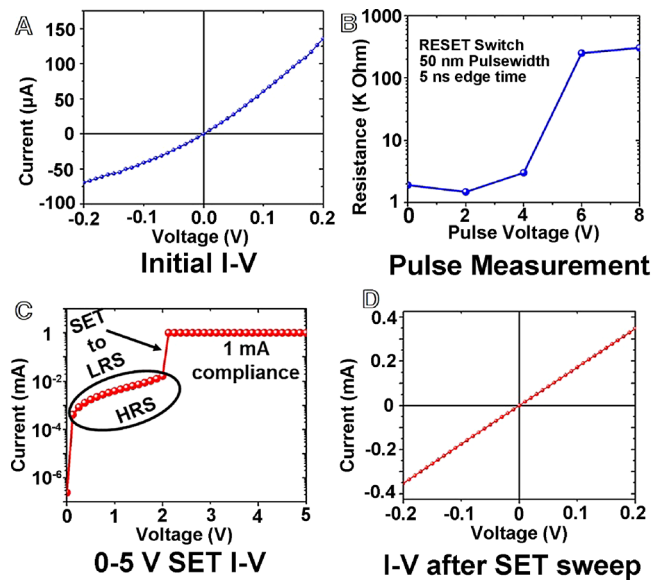


FIG. 2. (a) Initial I-V data show the electrical resistance of the nanosheet device in its initial LRS. (b) Device is subjected to a voltage pulsed with the 50 ns width and 5 ns edge times. A switch to the HRS is observed for pulse amplitudes greater than 6 V. (c) A high voltage I-V is performed to SET the device to the LRS, in line with the early experiments done by Waterman *et al.* A negative differential resistance is observed, indicating that the device returns to the original crystalline phase. (d) A low voltage I-V sweep confirms the return to the original crystalline phase. The small decrease in resistance and the increase in linearity of the I-V sweep over that in (a) can be attributed to contact annealing during pulsing.

To test whether the resistance switch is repeatable, we conducted pulse testing and measurements for the Sb_2Te_3 devices, as shown in Fig. 3(a). Besides the semiconductor analyzer, a B1530A module, an Agilent 3250A pulse generator unit, and an oscilloscope (Lecroy, WaveAce) were equipped. Figures 3(b) and 3(c) illustrate R-V characteristics of the nanosheet device under RESET pulses and SET pulses, respectively. The RESET pulses have the 10 ns pulse width and 10 ns edge time, whereas the SET pulses have a longer pulse width (100 μs) and edge time (100 μs). To evaluate the performance of nanosheet phase change memory, the device is cycled through RESET and SET pulses for 20 times. The resistance switching ratio (RSR) is 813 ± 168, nearly three orders of magnitude window between SET and RESET temperatures, starting in the amorphous phase, which is plotted in Fig. 3(e). Crystallization was observed starting at 360 K, and full crystallization indicated by a return to the LRS is found at 380 K. Figure 3(f) shows the device conductance under SET pulses of the increasing pulse width. These electrical characterization studies strongly indicate that resistance switching in these nanosheets is due to the crystalline-amorphous phase change under a melt quench mechanism. Sb_2Te_3 exhibits an unusual bonding mechanism favorable to glass formation. The amorphous state is reached through the application of a fast and high-energy thermal

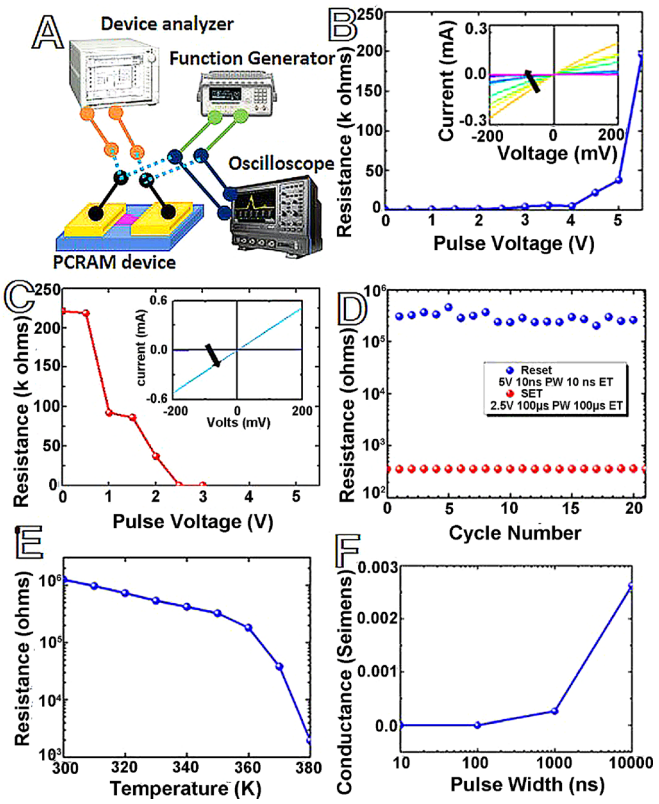
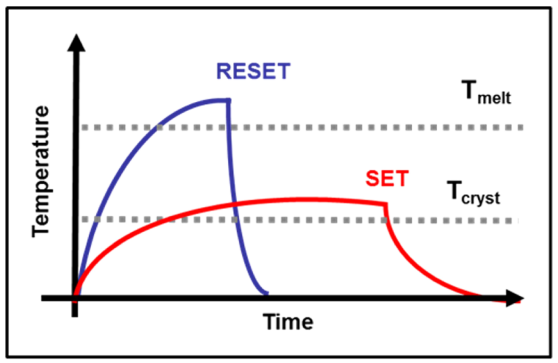
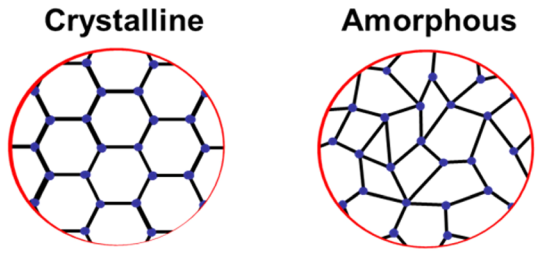


FIG. 3. (a) Custom built pulse measurement equipment for pulse testing and measurement of PCRAM devices. (b) R-V characteristics of the device under RESET pulses and (c) SET pulses. RESET pulses have the 10 ns pulse width and 10 ns edge time. SET pulses have a longer pulse width (100 μs) and edge time (100 μs). The insets of both (b) and (c) show the I-V data from which the R-V data are extracted. (d) RESET-SET cycling of the device. Repeated RESET-SET pulses were applied to the device to measure the RSR and cycling stability of the devices. (e) Resistance as a function of temperature starting in the amorphous phase. Crystallization was observed starting at 360 K, and full crystallization indicated by a return to the LRS is found at 380 K. (f) Graph showing the conductance of a device with SET pulses of the increasing pulse width. The minimum SET switching time found to be between 1 and 10 μs for the device.





Material Phase	Reflectivity (Optical)	Resistivity (Electrical)	Bit Value
Crystalline	High	Low	1
Amorphous	Low	High	0

FIG. 4. Schematic diagrams showing the operating principal of the phase-change material system under the melt-quench mechanism.

pulse that briefly brings the material above the melting point, as illustrated in Fig. 4. The application of thermal energy can bring the material above the melting temperature. If the material is cooled fast enough, it quenches it to an amorphous phase. The application of a lower-energy pulse results in a temperature above the crystallization point but below the melting point, bringing the material back to the thermodynamically favorable crystalline phase.

Whether the material reaches the glassy phase through a super-cooled liquid state,[20] or is driven to amorphization by the movement of ions via electrical wind-force,[21] is a matter of debate in the literature. It is agreed, however, that during the thermal pulsing, atoms in the material lose long-range order. When the thermal pulse is turned off sufficiently fast, the material quenches into a glassy amorphous state with low optical reflectivity and high electrical resistivity. While no external coolant is used to quench the material, the term quench is ubiquitously used to describe this phenomenon in phase change chalcogenides.[21–23] A longer, lower-energy pulse which raises the temperature above the crystallization point, but below the melting point, allows the material to return to the thermodynamically favorable crystalline phase with high reflectivity and low resistivity.[24]

The current, power, and energy as functions of time during the RESET switching data were also collected, as shown in Figs. 5(a)–5(c). The SET switching time was extracted by applying 2.5 V pulses with the logarithmically increasing pulse width and edge time. Current is extracted from the pulse voltage and LRS of the device as shown on top. The power is calculated from $P = IV$. The peak power during RESET switching is found to be $\sim 2.4 \times 10^{-2}$ W as shown in the middle image. Energy is extracted from integral over time of the power curve (the area under the power curve is highlighted in blue). The energy of the RESET switch is $< 3.4 \times 10^{-10}$ J as shown in the bottom image. Power dissipation during switching is estimated by the simple equality $P = V^2/R$, where P is the power, V is the voltage, and R is the resistance. Energy dissipation with error is calculated by taking the integral over time

$$E \pm \Delta E = \frac{1}{R}\int_0^t V^2 dt \pm \frac{2\Delta V}{R}\int_0^t V dt,$$

where E is the energy, ΔE is the variation, and t is the time. An estimation of the cell resistance value is necessary, as the testing methodology required to measure current during a nanosecond-time-domain voltage pulse has not been realized. This estimation was performed by applying Ohm's law to a current-voltage sweep of the device in the LRS, providing an upper bound of the power requirement. This upper bound estimation of power is valid as long as the cell increases its resistance value during switching to the HRS.

With the energy consumption information for each PCRAM device, we investigated the relationship between energy consumption and active layer thickness, as illustrated

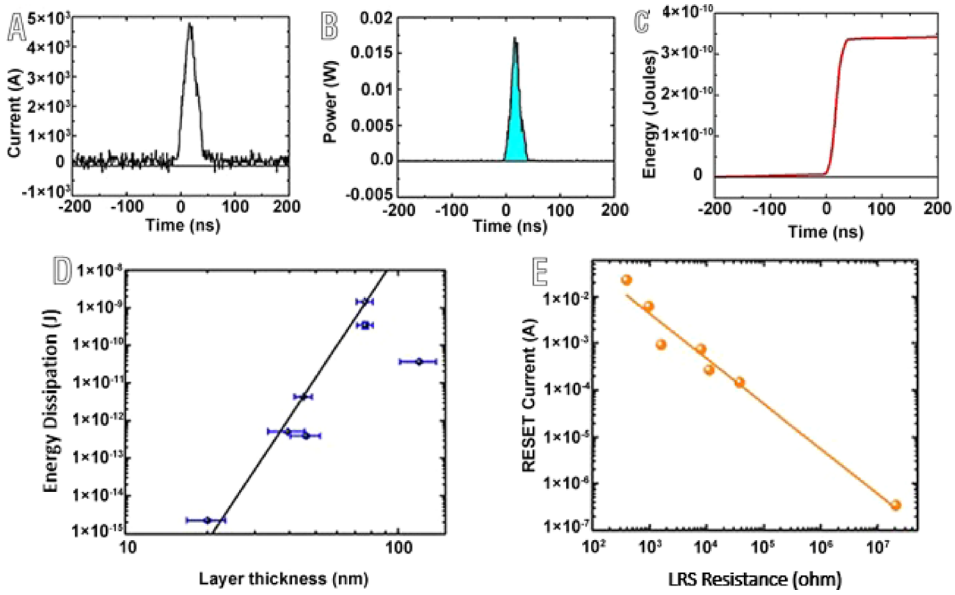


FIG. 5. The measured time-dependency of (a) electric current, (b) power, and (c) energy of a 2D nanosheet phase-change memory cell under the stimulation of a RESET pulse. (d) RESET energy consumption with respect to the nanosheet quintuple layer thickness. One quintuple layer is 1 nm thick, which corresponds to 1/3 of the traditional unit cell. Energy dissipation and error are calculated from the peak of the integral and noise floor of the pulse measurement. The thickness and error are calculated by measuring the heights of a region of the AFM image and comparing a region from the top of the contacts. (e) LRS state resistance measured in Ohms as a function of the RESET current at the peak of the pulse.

in Figs. 5(d) and 5(e). As the thickness of the nanosheet is scaled down to nanoscale dimensions, not only is the energy reduced due to less material volume but also the melting point, a critical factor in phase change memory operation, is significantly reduced according to previous studies on 1-D nanowires.[25,26] The energy dissipation with respect to the nanosheet thickness is found to have an exponential relationship. While the relationship is found to be approximately linear on a log-log scale, it is not assumed that this represents a power-law relationship, as many possible distributions are linear on such a scale.[27] The reduction in energy dissipation with the thickness represents a practical advantage over conventional thin-film phase change memory in terms of energy efficiency and device scalability. The exponential trend should continue with further dimensional scaling, but the ultimate scaling limit for the antimony telluride phase-change material in the direction parallel to the crystallographic c-axis is one quintuple layer (~1 nm thick or one-third of the traditional unit cell). Previous solutions for scaling phase change memory include using a nanowire based phase-change memory,[28] self-aligned nanotubes as electrical contacts,[29,30] and confinement within a nanotube.[31] While the performance metrics of 2D chalcogenide nanosheet phase change memory presented here are anticipated to fall between that of the thin-film "mushroom cap" and the more exotic 1D structures, employing a 2D nanosheet may prove to be the most practical path towards ultimately scalable phase-change systems, as the "super-thin-film" could be grown via viable material processes such as chemical vapor deposition or atomic layer deposition. Top-down approaches may be utilized to confine the lateral dimensions of the nanosheets, leading to the realization of 2D material-based phase change device arrays for a range of applications including high-capacity data storage and artificial neural networks.

To summarize, we have demonstrated resistive switching behavior in 2D layered Sb_2Te_3 nanosheets. The observed repeatable HRS-LRS switching under externally applied electrical pulses is due to the structural transition between crystalline and amorphous phases under a melt-quench-recrystallization mechanism. The energy required to amorphize the nanosheets is observed to decrease exponentially with the reduced physical layer thickness, indicating the potential benefit in ultra-scaled phase-change material systems. Pushing to the two-dimensional limit in chalcogenide phase-change devices could lead to the implementation of those basic building elements for the next-generation computing systems, including non-volatile memories and programmable logic and neurobiological devices with very high energy-efficiency.

See supplementary material for the figure showing the indexed X-ray diffraction spectrum of an ensemble of Sb_2Te_3 nanosheets exfoliated on a silicon surface.

We acknowledge funding support from the National Science Foundation (Grant Nos. 1162312 and 1434689).

[1]A. T. Waterman, London, Edinburgh, Dublin Philos. Mag. J. Sci. **33**, 225–247 (1917).
[2]S. R. Ovshinsky, "Reversible electrical switching phenomena in disordered structures," Phys. Rev. Lett. **21**, 1450 (1968).
[3]A. A. Bessonov, M. N. Kirikova, D. I. Petukhov, M. Allen, T. Ryhänen, and M. J. Bailey, "Layered memristive and memcapacitive switches for printable electronics," Nat. Mater. **14**, 199–204 (2015).
[4]X. Tao and Y. Gu, "Crystalline-crystalline phase transformation in two-dimensional In_2Se_3 thin layers," Nano Lett. **13**, 3501–3505 (2013).
[5]B. Radisavljevic, A. Radenovic, J. Brivio, V. Giacometti, and A. Kis, "Single-layer MoS_2 transistors," Nat. Nanotechnol. **6**, 147–150 (2011).
[6]Y. M. Lin, C. Dimitrakopoulos, K. A. Jenkins, D. B. Farmer, H. Y. Chiu, A. Grill, and P. Avouris, "100-GHz transistors from wafer-scale epitaxial graphene," Science **327**, 662–662 (2010).
[7]Z. Zhang, F. Yang, P. Agnihotri, J. U. Lee, and J. R. Lloyd, "Reverse degradation of nickel graphene junction by hydrogen annealing," AIP Adv. **6**, 025301 (2016).
[8]N. Jain, M. Murphy, R. B. Jacobs-Gedrim, M. Shanmugam, F. Yang, E. Sang, and B. Yu, "Electrical conduction and reliability in dual-layered graphene heterostructure interconnects," IEEE Electron Device Lett. **35**, 1311–1313 (2014).
[9]M. L. Tsai, S. H. Su, J. K. Chang, D. S. Tsai, C. H. Chen, C. I. Wu, L. J. Li, L. J. Chen, and J. H. He, "Monolayer MoS_2 heterojunction solar cells," ACS Nano **8**, 8317–8322 (2014).
[10]F. H. L. Koppens, T. Mueller, P. Avouris, A. C. Ferrari, M. S. Vitiello, and M. Polini, "Photodetectors based on graphene, other two-dimensional materials and hybrid systems," Nat. Nanotechnol. **9**, 780–793 (2014).
[11]D. Sarkar, W. Liu, X. Xie, A. C. Anselmo, S. Mitragotri, and K. Banerjee, "MoS_2 field-effect transistor for next-generation label-free biosensors," ACS Nano **8**, 3992–4003 (2014).

[12]Y. Liu, X. Dong, and P. Chen, "Biological and chemical sensors based on graphene materials," Chem. Soc. Rev. **41**, 2283–2307 (2012).
[13]K. NDri, J. Sei, D. Houphouet-Boigny, G. Kra, and C. J. Jumas, "Estimation of glass-forming ability and glass stability of Sb_2S_3-As_2S_3-Sb_2Te_3 glasses by thermal properties," J. Appl. Sci. **7**, 3167–3176 (2007).
[14]A. L. Lacaita and A. Redaelli, "The race of phase change memories to nanoscale storage and applications," Microelectron. Eng. **109**, 351–356 (2013).
[15]Y. Li, Y. P. Zhong, Y. F. Deng, Y. X. Zhou, L. Xu, and X. S. Miao, "Nonvolatile "AND," "OR," and "NOT" Boolean logic gates based on phase-change memory," J. Appl. Phys. **114**, 234503 (2013).
[16]B. L. Jackson, B. Rajendran, G. S. Corrado, M. Breitwisch, G. W. Burr, R. Cheek, K. Gopalakrishnan, S. Raoux, C. T. Rettner, A. Padilla *et al.*, "Nanoscale electronic synapses using phase change devices," ACM J. Emerging Technol. Comput. Syst. (JETC) **9**(2), 12 (2013).
[17]F. Yang, R. B. Jacobs-Gedrim, M. Shanmugam, N. Jain, M. T. Murphy, E. S. Song, D. Frey, and B. Yu, "Scalable synthesis of two-dimensional antimony telluride nanoplates down to a single quintuple layer," RSC Adv. **5**, 59320–59325 (2015).
[18]F. Yang, M. Sendova, R. B. Jacobs-Gedrim, E. S. Song, A. Green, P. Thiesen, A. Diebolt, and B. Yu, "Rapid optical determination of topological insulator nanoplate thickness and oxidation," AIP Adv. **7**, 015114 (2017).
[19]J. S. Lee, S. Brittman, D. Yu, and H. Park, "Vapor-liquid-solid and vapor-solid growth of phase-change Sb_2Te_3 nanowires and Sb_2Te_3/GeTe nanowire heterostructures," J. Am. Chem. Soc. **130**, 6252–6258 (2008).
[20]A. Sebastian, M. Le Gallo, and D. Krebs, "Crystal growth within a phase change memory cell," Nat. Commun. **5**, 54314 (2014).
[21]S. W. Nam, H. S. Chung, Y. C. Lo, L. Qi, J. Li, Y. Lu, A. C. Johnson, Y. Jung, P. Nukala, and R. Agarwal, "Electrical wind force-driven and dislocation-templated amorphization in phase-change nanowires," Science **336**, 1561–1566 (2012).
[22]S. Raoux and M. Wuttig, *Phase Change Materials* (Springer Science & Business Media, 2010).
[23]M. Wuttig and N. Yamada, "Phase-change materials for rewriteable data storage," Nat. Mater. **6**, 824–832 (2007).
[24]R. Jeyasingh, S. W. Fong, J. Lee, Z. Li, K. W. Chang, D. Mantegazza, M. Asheghi, K. E. Goodson, and H. S. P. Wong, "Ultrafast characterization of phase-change material crystallization properties in the melt-quenched amorphous phase," Nano Lett. **14**, 3419–3426 (2014).
[25]X. Sun, B. Yu, G. Ng, and M. Meyyappan, J. Phys. Chem. C **111**, 2421–2425 (2007).
[26]J. Liu, B. Yu, and M. P. Anantram, IEEE Electron Device Lett. **32**, 1340–1342 (2011).
[27]A. Clauset, C. R. Shalizi, and M. E. Newman, "Power-law distributions in empirical data," SIAM Rev. **51**, 661–703 (2009).
[28]B. Yu, X. Sun, S. Ju, D. B. Janes, and M. Meyyappan, "Chalcogenide-nanowire-based phase change memory," IEEE Trans. Nanotechnol. **7**, 496–502 (2008).
[29]J. Liang, R. G. D. Jeyasingh, H. Y. Chen, and H. S. P. Wong, "An ultra-low reset current cross-point phase change memory with carbon nanotube electrodes," IEEE Trans. Electron Devices **59**, 1155–1163 (2012).
[30]F. Xiong, A. D. Liao, D. Estrada, and E. Pop, "Low-power switching of phase-change materials with carbon nanotube electrodes," Science **332**, 568–570 (2011).
[31]C. E. Giusca, V. Stolojan, J. Sloan, F. Börrnert, H. Shiozawa, K. Sader, M. H. Rümmeli, B. Büchner, and S. R. P. Silva, "Confined crystals of the smallest phase-change material," Nano Lett. **13**, 4020–4027 (2013).